APPLICATION OF ELECTROCHEMICAL IMPEDANCE SPECTROSCOPY TO THE STUDY OF SURFACE PROCESSES

Manuela Rueda Rueda[1] and Francisco Prieto Dapena[2,*]

Department of Physical Chemistry, Faculty of Pharmacy, University of Sevilla, C. Profesor García González 2, 41012 Sevilla, Spain; e-mail: [1] marueda@us.es, [2] dapena@us.es

Received June 8, 2011
Accepted August 22, 2011
Published online January 23, 2012

This work is dedicated to Dr Lubomír Pospíšil on the occasion of his 70th birthday in recognition of his outstanding contribution to electrochemistry.

The application of Electrochemical Impedance Spectroscopy to the study of surface electrode processes is reviewed. The impedance expressions and the physical meaning of the parameters included in them are shown for three surface processes: adsorption kinetics, diffusion towards partially blocked electrodes and surface confined redox reactions. The models are applied to selected examples, showing the capability of Electrochemical Impedance Spectroscopy to obtain fundamental kinetic information of these processes. A review with 83 references.

Keywords: Electrochemistry; Adsorption; Kinetics; Ion channels; Electron transfer; Surface processes; EIS.

1. INTRODUCTION

Surface reactions occurring at electrodes are receiving great attention by scientist of different fields: material science, corrosion, energy storage and conversion, electrocatalysis, sensors or bioelectrochemistry among others, either because of the inherent interest of the surface electrode process or because the electrode surface constitutes a suitable model for the system of interest.

Electrochemical dc techniques have been more widely applied, as compared to ac current techniques, to this kind of studies. They permit to get a rapid set of data that can be used to build a rough picture of the process and to determine some thermodynamic and kinetic parameters and/or structural information.

However, the information provided by electrochemical dc measurements is limited by different factors. The data obtained in a classical electrochemi-

Collect. Czech. Chem. Commun. 2011, Vol. 76, No. 12, pp. 1825–1854

doi:10.1135/cccc2011118

cal experiment may include contributions from several phenomena: double layer charge, mass transport, adsorption, electrode processes including electron transfers, heterogeneous and homogeneous chemical reactions. In the study of one specific phenomena, the time window accessible will be limited by the rate of the other phenomena contributing to the overall signal. For instance, in electrode kinetic studies, the higher rate constant values that can be measured use to be limited by the rate of mass transport. Electrochemical dc methods that decrease the characteristic time of mass transport (fast voltammetry, chronomethods, ultramicroelectrodes, forced convection, etc.) permit to extend the upper limit of measurable rate constants values. For extreme rate of mass transport the limitations would be imposed by the double layer phenomena.

Electrochemical Impedance Spectroscopy (EIS) has the capability to separate the different contributions to the electrochemical response of the interface thus constituting a powerful method to overcome some of the limitations indicated above in the study of electrode kinetics. Experimentally, a small amplitude ac signal is superimposed to the dc potential perturbation applied to the electrochemical cell, and the ac current response is related to the ac potential perturbation. The analysis of the impedance data as a function of the ac frequency, according to a suitable model, can provide quantitative parameters of the electrode process. The behaviour of these parameters with the dc potential can be used to reach a deeper characterization of the electrode processes[1–3]. In this way the Electrochemical Impedance Spectroscopy has been applied to the kinetic and mechanistic study of electrode reactions of organic compounds. Sequential and parallel multistep mechanisms with homogeneous or heterogeneous chemical steps, stable intermediates, weak adsorption of reactant and or product, etc, have been addressed[4–11].

The frequency spectrum performed at a single potential is often employed to characterize complex electrode surface situations: corrosion, self-assembled monolayers, etc. The results obtained are analyzed according to equivalent circuits, sometimes without a clear correlation with the physical meaning of the system. The information obtained from this kind of procedure cannot be straightforward related to a quantitative physical model.

However, the electrochemical impedance spectra obtained as a function of the dc potential, and their analysis both with the frequency and with the potential, according to the equations deduced for a proposed model can provide a direct evidence of the suitability of the model, and quantitative information can be obtained. In the literature there are excellent contributions about the application of EIS to kinetic and mechanistic studies of elec-

trode processes[4–11]. However less attention has been paid to the study of surface processes by impedance methods.

In this paper, the application of EIS to three specific surface processes is shown: adsorption kinetics of organic molecules on single crystal electrodes, faradaic reactions at partially blocked electrodes and surface confined electrode reactions. The impedance equations corresponding to these surface processes are explained and applied to one model-system of each kind of surface process: the kinetics of adenine adsorption on Au(111) electrodes, Tl(I) reduction on gramicidin modified phospholipids coated mercury electrodes and, finally, the reduction of azobenzene on mercury electrodes.

2. KINETICS OF THE ADSORPTION OF ORGANIC COMPOUNDS ON SINGLE CRYSTAL ELECTRODES

Electrochemical studies of the adsorption of organic compounds on metal electrodes usually consider the electrified interface as a series RC equivalent circuit. However, many experimental situations do not exhibit the expected behaviour for the series RC circuit, showing capacity dispersion with frequency. That dispersion has been ascribed either to geometric effects of the electrode roughness, or to the heterogeneity of the electrode surface or to interfacial phenomena such as interphase reorganization, dielectric relaxation of solvent or slow adsorption processes[12,13].

In the case of single crystal electrodes the surface exposed to the solution is smooth and, therefore, the dispersion of the capacity with frequency cannot be a consequence of geometric effects of the roughness. Moreover, deviations from the expected behavior for an RC circuit are more evident in the case of specific adsorption of organic molecules or anions present in the solution[14–16]. These deviations have been explained as a consequence of the kinetics limitations of the adsorption process.

The first kinetic model was developed by Frumkin and Melik–Gaikazyan[17] for the adsorption of alcohols on mercury electrodes. This model considers two limiting cases, corresponding to pure kinetic control by the transport step or by the adsorption step. In addition, the model assumes a Butler–Volmer type potential dependence of the rate constant of the adsorption step and a Langmuir relationship for the adsorbate concentration.

The model has been applied to the adsorption of camphor on mercury electrodes by Retter and Jehring[18], and to the adsorption of organic compounds on bismuth single crystals[19] by Berzins and Delahay, who have extended the model to include possible mixed kinetic control either by mass

transport and adsorption steps. Recently, the original model has been modified eliminating the "a priori" assumption about the rate equation of the adsorption step, which in the original model was a Langmuir equation, and applied to the adsorption of anions on gold single crystal electrodes[20–23].

2.1. The Adsorption Impedance

In the presence of specific adsorption the charge density on the electrode surface (σ^M) can be considered a function of the dc potential (E) and of the surface excess (Γ). Therefore, the variation of the charge density with time can be expressed as:

$$\frac{d\sigma^M}{dt} = j = \left(\frac{\partial\sigma^M}{\partial E}\right)_\Gamma \frac{dE}{dt} + \left(\frac{\partial\sigma^M}{\partial\Gamma}\right)_E \frac{d\Gamma}{dt} \,. \tag{1}$$

Where the current density (j) includes two contributions. The first one is a capacitative component, caused by the double layer charge process including the adsorbate molecules:

$$j_c = \left(\frac{\partial\sigma^M}{\partial E}\right)_\Gamma \frac{dE}{dt} = C_d \frac{dE}{dt} \,. \tag{2}$$

With C_d being de double layer capacity.

The second contribution depends on the adsorption rate:

$$j_{ad} = \left(\frac{\partial\sigma^M}{\partial\Gamma}\right)_E \frac{d\Gamma}{dt} = \left(\frac{\partial\sigma^M}{\partial\Gamma}\right)_E v \,. \tag{3}$$

The net rate of adsorption, v, can be defined:

$$v = \frac{d\Gamma}{dt} = k_{ad} f_{ad}(\Gamma) c_{x=0} - k_d f_d(\Gamma) \,. \tag{4}$$

Where k_{ad} and k_d are the rate constants of adsorption and desorption steps, respectively, and $f_{ad}(\Gamma)$ and $f_d(\Gamma)$ are respectively decreasing and increasing monotonic functions of the surface excess, Γ, related to the adsorption isotherm. The values of the functions $f_{ad}(\Gamma)$ and $f_d(\Gamma)$ tend to 1 and 0, respectively when the surface excess tends to 0. On the other side, when the

surface excess approximates to its maximum value (Γ_m) $f_{ad}(\Gamma)$ and $f_d(\Gamma)$ tend to 0 and 1, respectively.

The instant adsorption rate, is a function of the concentration of adsorbate at the electrode neighborhood, of the surface excess and of the potential applied. Under a small amplitude perturbation the response can be considered linear. Changing to the Laplace space and including the second Fick's law for linear diffusion, the solution of the mass transport problem can be straightforward obtained for semi-infinite diffusion boundary conditions. Then, the expression for the adsorption impedance can be obtained[23,24]:

$$Z_{ad} = R_{ad} + \frac{\sigma_{ad}}{(i\omega)^{1/2}} + \frac{1}{C_{ad} i\omega} . \tag{5}$$

Where i is the complex unit $(-1)^{1/2}$ and ω is the angular frequency.

Equation (*5*) includes three different terms whose frequency dependence corresponds respectively to a resistance, to a Warburg element and to a capacitance. The coefficients included in these terms can be named adsorption resistance (R_{ad}), adsorption Warburg coefficient (σ_{ad}) and adsorption capacitance (C_{ad}). Their definitions are given in Eqs (*6*) to (*8*):

$$R_{ad} = \left(\frac{\partial I_{ad}}{\partial E} \right)^{-1}_{c,\Gamma} \tag{6}$$

$$\sigma_{ad} = -\frac{1}{D^{1/2} \gamma F} \left(\frac{\partial I_{ad}}{\partial E} \right)^{-1}_{c,\Gamma} \left(\frac{\partial I_{ad}}{\partial c} \right)_{E,\Gamma} \tag{7}$$

$$C_{ad} = \gamma F \left(\frac{\partial I_{ad}}{\partial \Gamma} \right)^{-1}_{E,c} \left(\frac{\partial I_{ad}}{\partial E} \right)_{c,\Gamma} . \tag{8}$$

The impedance of the cell includes also the ohmic resistance, R_S, and a double layer capacity, C_d, defined as:

$$C_d = \left(\frac{\partial \sigma^M}{\partial E} \right)_{\Gamma} . \tag{9}$$

Therefore, the impedance of the electrochemical cell can be expressed:

$$Z_{cel} = R_s + \frac{1}{C_d i\omega + \dfrac{1}{R_{ad} + \dfrac{\sigma_{ad}}{(i\omega)^{1/2}} + \dfrac{1}{C_{ad} i\omega}}} . \qquad (10)$$

Equation (*10*) shows the same frequency dependence of the impedance as that of the electrical circuit in Scheme 1.

From the definitions of the parameters R_{ad} and σ_{ad}, Eqs (*6*) and (*7*), and taking into account Eqs (*3*) and (*4*), the ratio σ_{ad}/R_{ad} can be related to the apparent rate constant of the adsorption process:

$$\sqrt{D}\,\frac{\sigma_{ad}}{R_{ad}} = k_{ad} f_{ad}(\Gamma) \qquad (11)$$

On the other hand, Eqs (*6*) and (*7*) can be transformed in order to obtain a more explicit meaning of the parameters R_{ad} and σ_{ad}. Assuming that under an infinitesimal perturbation of the adsorption equilibrium the response (j_{ad}) will be proportional to the magnitude of the adsorption driving force:

$$j_{ad} \propto (\mu_s - \mu_{ad}) . \qquad (12)$$

Where μ_s and μ_{ad} are the chemical potentials of the adsorbate in solution and in adsorbed state, respectively. Considering that μ_{ad} is only a function of the surface excess, Γ, and the dc potential, *E*, and:

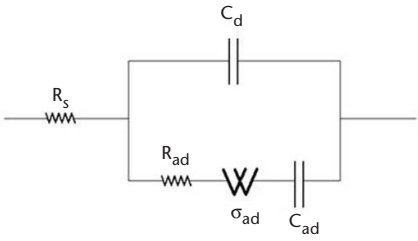

SCHEME 1
Equivalent circuit representing the electrochemical cell with an adsorption impedance according to Eq. (*5*). With permission from *Electrochim. Acta* **2010**, *55*, 3301

$$\mu_s = \mu_s^0 + RT \ln c \tag{13}$$

Equation (*7*) can be transformed in:

$$\sigma_{ad} = \frac{RT}{\gamma^2 F^2 c\sqrt{D}} \tag{14a}$$

and, from Eq. (*10*):

$$R_{ad} = \frac{RT}{\gamma^2 F^2 c\, k_{ad} f_{ad}(\Gamma)} \,. \tag{14b}$$

Where γ is the electrosorption valency.

These expressions show that R_{ad} depends on the apparent rate constant of the adsorption process while σ_{ad} values are affected by the diffusion coefficient.

From Eqs (*6*)–(*8*) the relaxation times of diffusion, τ_D, and adsorption, τ_H, are obtained:

$$2^{-1/2} \sigma_{ad} C_{ad} = -(2D)^{-1/2} \left(\frac{\partial \Gamma}{\partial c} \right)_E = \tau_D^{1/2} \tag{15a}$$

$$R_{ad} C_{ad} = \left(\frac{\partial \Gamma}{\partial v} \right)_{E,c} = \tau_H \tag{15b}$$

The frequency analysis of the impedance spectra according to Eq. (*5*) provides the values of R_{ad}, σ_{ad} and C_{ad} at every dc potential. These values permit to obtain the kinetic parameters of the model and their potential dependence.

2.2. Example 1: The Adsorption of Adenine on Au(111)

The adsorption of adenine on Au(111) and (100) from NaF solutions was characterized by Rueda et al.[25] by means of cyclic voltammetry, single frequency capacitance and chronoamperometric measurements in 0.5 M NaF solutions.

In the capacitance–potential plots adenine adsorption shows up as a capacitance peak at the more negative potentials and a flat low capacitance region at more positive potentials (Fig. 1).

The kinetics of the adsorption process was studied by impedance spectroscopy measurements at several dc potentials along the capacitance peak and the results were analyzed according to the model described in the previous section[26].

The complex plane impedance plots obtained in the presence of adenine show clear deviations from the RC type behaviour. These deviations cannot be caused by surface roughness because the Nyquist plots obtained in the absence of adenine correspond to a pure capacitative behaviour. Therefore, the influence of the adenine adsorption kinetics can be inferred from these plots.

More straightforward characterisation can be observed in the admittance plots. The frequency dependence of the real and imaginary components of the electrode admittance, Y_{el}' and Y_{el}'', can be represented by the plots Y_{el}'/ω vs Y_{el}. The plots are arc-shaped intercepting the Y_{el}''/ω axis at the $C_{dl,\Gamma}$ and $C_{dl,\Gamma} + C_{ad}$ values at low and at high frequencies, respectively. In the limiting case of pure adsorption kinetic control, the resulting arcs are

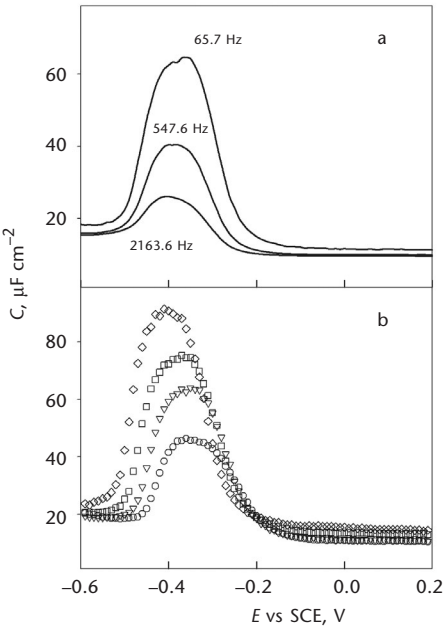

FIG. 1
C vs *E* plots obtained (a) at the indicated ac frequencies in 1 mM adenine solutions in NaF 0.5 M and (b) at 21.9 Hz for 0.5 NaF solutions containing adenine 0.1 mM (○), 0.5 mM (△), 1 mM (□) and 5 mM (◇). With permission from *Electrochim. Acta* **2010**, *55*, 3301

perfect semicircles while in the limiting case of pure diffusion control depressed arcs appear. If both steps contribute to the kinetic control, skewed intermediate arcs are obtained[23,24]. Most of the arcs obtained for adenine adsorption on Au(111) are representative of mixed kinetic control at potentials close to the adsorption-desorption capacitance peak. At more positive potentials the adsorption is so fast that no deviations from the RC behaviour are observed.

The electrode admittance components, Y_{el}' and Y_{el}, for the system can be theoretically deduced from Eq. (*10*) after splitting the cell impedance into its components and proper recombination[26]. The frequency analysis of the experimental Y_{el}' and Y_{el}'' values according to the theoretical expressions provides the values of R_{ad}, σ_{ad}, C_{ad} and C_d at every dc potential.

C_{ad} vs E and C_d vs E plots are shown in Fig. 2. C_d is approximately coincident to the double layer capacitance measured in the absence of adenine at potentials more negative that the pseudocapacitance peak in Fig. 1. At more positive potentials C_d becomes lower than the supporting electrolyte capacitance. C_{ad} vs E plots exhibit a peak that shifts towards more negative potentials with increasing adenine concentration.

Plots of the parameters R_{ad} and σ_{ad} vs E are shown in Figs 3a and 3b, respectively. R_{ad} values are at least two orders of magnitude lower than σ_{ad}. This fact, under the range of frequencies used, involves that the second addend in Eq. (*5*) including the Warburg coefficient has a more important

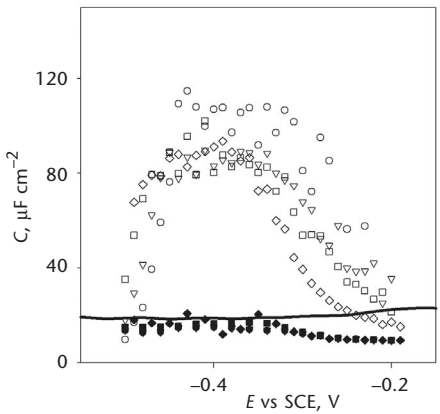

FIG. 2

C_d vs E (filled symbols) and C_{ad} vs E (hollow symbols) obtained from the analysis with the frequency for 0.5 NaF solutions containing adenine. Symbols as in Fig. 1. The line corresponds to the pseudo capacitance data obtained in the absence of adenine at 21.9 Hz. With permission from *Electrochim. Acta* **2010**, *55*, 3301

contribution to the adsorption impedance, than the adsorption resistance. R_{ad} vs E plots are higher as adenine concentration decreases and tend to be coincident for different adenine concentrations at the more negative potentials.

From the C_{ad}, R_{ad} and σ_{ad} values at every dc potential and adenine concentration the relaxation times of adsorption and diffusion can be obtained using Eqs (*15a*) and (*15b*). The τ_D values range from 0.3 to 30 ms, depending on adenine concentration and potential. However, the adsorption relaxation time is about 10 times shorter than the diffusion relaxation time. Therefore, mixed kinetics with lower contribution of the adsorption step can be inferred. From the combination of R_{ad} and σ_{ad} values according to Eq. (*11*) the specific rate of adsorption, $k_{ad}f_{ad}(\Gamma)$, was obtained at every potential. In Fig. 4a the rate constant values are plotted against the potential for the case of adenine adsorption from 5×10^{-4} mol l^{-1} solutions. It can be

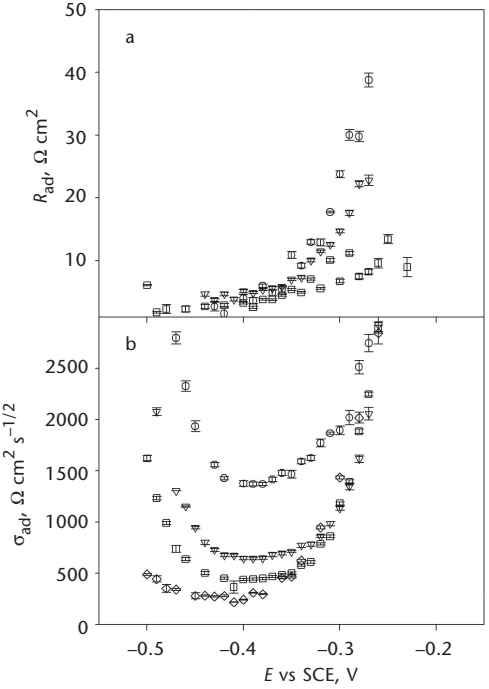

FIG. 3
R_{ad} vs E (a) and σ_{ad} vs E (b) plots obtained from the analysis with the frequency for 0.5 M NaF solutions containing adenine. Symbols as in Fig. 1. With permission from *Electrochim. Acta* **2010**, *55*, 3301

observed that $k_{ad}f_{ad}(\Gamma)$ decreases if the potential increases. This behaviour can be explained taking into account that the surface excess increases with the potential and that $f_{ad}(\Gamma)$ is a monotonically decreasing function of Γ. The net potential behaviour of $k_{ad}f_{ad}(\Gamma)$ is the balance between the expected increasing Butler–Volmer behaviour of k_{ad} and the decreasing behaviour of $f_{ad}(\Gamma)$.

In order to obtain the explicit expression for $f_{ad}(\Gamma)$ it is necessary to assume an adsorption isotherm. In the thermodynamic study of the adsorption of adenine on Au(111)[25] the experimental data were explained

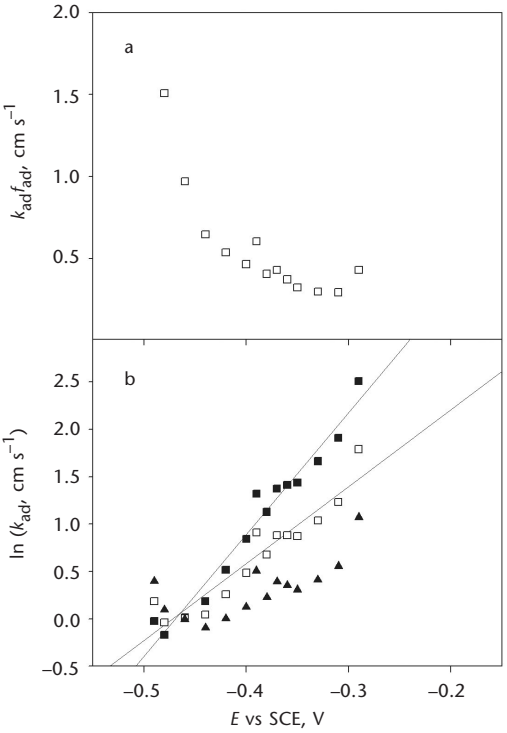

FIG. 4

(a) Adsorption specific rate vs potential obtained using Eq. (*11*) and the values of R_{ad} and σ_{ad} from the analysis with the frequency for 1 mM adenine in aqueous 0.5 M NaF. (b) Natural logarithm of the adsorption rate constant (k_{ad}) calculated from adsorption specific rate and the values of $f_{ad}(\Gamma)$ calculated conforming to a Frumkin isotherm with the data in ref.[15] and considering $(g^{\neq}/g) = 1$ (■), 0.75 (□) and 0.5 (▲). The solid lines are the linear regressions to the data with $(g^{\neq}/g) = 1$ and $(g^{\neq}/g) = 0.75$. With permission from *Electrochim. Acta* **2010**, *55*, 3301

according to a Frumkin isotherm with negative values for the interaction parameter (g), suggesting unstable adsorbate–adsorbate interactions as compared to adsorbate–solvent interactions. Szulborska and Baranski[27] suggested that these situations involves that either the adsorption and the desorption steps have an energy barrier that includes the energy of the lateral interaction between the "activated complex" and the adsorbate molecule in its ground state. The dependence of $k_{ad}f_{ad}(\Gamma)$ with the potential has been explained[25] assuming an interaction parameter for the "activated complex" ($g^{\neq}$) similar to the interaction parameter for the adsorbate molecule in its ground state. Then the behaviour obtained for the adsorption rate constant with the potential is consistent with the expected Butler–Volmer behaviour, as can be observed in Fig. 4b.

3. DIFFUSION TOWARDS PARTIALLY BLOCKED ELECTRODES

Coverage of the electrode surface by organic films may block ionic and electronic transfers between the solution and the electrode. Defects into this insulating film may act as active pinholes surrounded by inactive areas. Depending on the size of the active pinholes and the distance between them, each individual pinhole behaves as an individual ultramicroelectrode with its own diffusion profile that could contain radial contributions. Examples of non-linear diffusion effects can be found in the electrodes covered by electroactive or electroinactive polymer films, or in the ionic transport trough biological membranes.

3.1. Electrochemical Impedance of Partially Blocked Electrodes

Vetter[28] deduced the impedance equations for these systems and they were applied by Retter et al.[29] to the reduction of Tl(I) ions on mercury electrodes covered by some organic films. Matsuda and coworkers[30] considered the nonlinear contributions to the diffusion towards macroscopic inhomogeneities and deduced the equations for the impedance of a redox process. Amatore et al.[31] developed a model for an electrode surface including 'active' disks dispersed on an insulating film and deduced the corresponding voltammetric equations for the case of very low active sites coverage. The model extended to more general non linear diffusion systems has received great attention and it has been applied to several experimental systems[32–35].

The faradaic impedance equations for Amatore's model[31] were first obtained by Finklea et al.[36]. The expressions for real and imaginary compo-

nents of the faradaic impedance (Z_F' and Z_F'', respectively) as a function of the angular frequency (ω) are:

$$Z_F' = \frac{R_{ct}}{1-\theta} + \frac{\sigma}{\omega^{1/2}} + \frac{\sigma}{1-\theta}\left[\frac{(\omega^2 + q^2)^{1/2} + q}{\omega^2 + q^2}\right]^{1/2} \tag{16a}$$

$$Z_F'' = \frac{\sigma}{\omega^{1/2}} + \frac{\sigma}{1-\theta}\left[\frac{(\omega^2 + q^2)^{1/2} - q}{\omega^2 + q^2}\right]^{1/2} . \tag{16b}$$

Where (1 – θ) is the coverage of active sites, σ and R_{ct} have their usual meanings, and q is a parameter depending on the size of the active centres. The model represents either the active sites or the inactive domains surroundings as discs of radio R_a and R_0 respectively. q is then given by Eq. (*17a*) and the coverage of the blocking layer, θ, is obtained from R_a and R_0 as is shown in Eq. (*17b*).

$$q = \frac{D}{0.36R_a^2} \tag{17a}$$

$$1 - \theta = \frac{R_a^2}{R_0^2} \tag{17b}$$

The diffusion coefficient (D) has been considered to be the same for the oxidised and the reduced forms of the redox couple.

From the frequency dependence of Z_F' and Z_F'' in Eq. (*16*), two pseudo-Randless limiting cases can be inferred, at low and at high frequencies. These limiting cases can be easily detected by means of the plots of Z_F' or Z_F'' vs $\omega^{-1/2}$, which exhibit two characteristic linear sections corresponding to the pseudo-Randles limiting cases. The high frequency limit ($\omega >> q$) corresponds to nearly isolated diffusion profiles, while the low frequency limit ($\omega << q$) corresponds to overlapping diffusion profiles for all the active centres.

In general, a pseudo-Randles case involves the same frequency dependence than a "true" Randles behaviour, but with different meanings for R_{ct} and σ than those for a simple electron transfer[11]. For the limiting cases described above, the meanings of R_{ct} and σ are[36]:

High frequency limit ($\omega >> q$)

$$(R_{ct})_{app} = \frac{R_{ct}}{1-\theta} \tag{18a}$$

$$(\sigma)_{app} = \sigma\left(1 + \frac{1}{1-\theta}\right). \tag{18b}$$

Low frequency limit ($\omega << q$)

$$(R_{ct})_{app} = \frac{R_{ct}}{1-\theta} + \frac{\sigma R_a \left(\frac{0.72}{D}\right)^{1/2}}{1-\theta} \tag{19a}$$

$$(\sigma)_{app} = \sigma\ . \tag{19b}$$

The slopes of Z_F' or Z_F'' vs $\omega^{-1/2}$ correspond to $(\sigma)_{app}$ and, therefore, have to be the same for the two impedance components at each limiting case. Taking into account Eqs (*18b*) and (*19b*), the ratio between the slopes at the high and the low frequency limits allows the evaluation of the coverage, Eq. (*20a*). The frequency of the intersection of the two limiting pseudo-Randles cases can be used to calculate the radio of the active pinholes, Eq. (*20b*).

$$\frac{\text{slope high frequency}}{\text{slope low frequency}} = \frac{2-\theta}{1-\theta} \tag{20a}$$

$$\omega_{\text{intercept}} = \frac{q}{2} = \frac{D}{0.72R_a^2}\ . \tag{20b}$$

3.2. Example: Gramicidin Modified Phospholipid Coated Mercury Electrodes

Phospholipid coated mercury electrodes were first introduced by Miller[37] and later extensively developed by Nelson et al.[38–48]. These electrodes were used as model systems to study ion and electron transfers in biological membranes by electrochemical methods. It consists of a monolayer of

phospholipid molecules oriented with the polar heads towards the solution.

In the case of dioleoylphosphatidylcholine (DOPC) the monolayer is impermeable to inorganic anions on a wide potential range, at least from –0.2 to –0.6 V vs SCE, characterized by a low and potential independent capacitance value. However, at more negative potentials, around –0.9 V vs SCE, the phospholipid molecules modify their orientation, forming defects that permit the permeation of inorganic species from solution. Moreover, in the presence of gramicidin, a forming channels peptide[49–51], the transport of monovalent cations across the monolayer can be studied.

The reduction of Tl(I) ions on bare mercury takes place at potentials at which the DOPC monolayer is impermeable to the cations, so the signal obtained with gramicidin-modified DOPC coated mercury electrodes is due to the reduction of Tl^+ through the gramicidin channels. This reduction has been extensively studied by several electrochemical methods[41–48,52–55], but the results cannot be described by a single electron transfer with linear diffusion, as applies for the Tl(I) reduction on bare mercury[56,57]. Different mechanistic schemes including homogeneous and heterogeneous chemical steps have been proposed[41,42,46,48,52,54,55] to explain the results obtained although the physical meaning of the chemical steps is not clear. On the other hand, the mass transport equations describing the system with homogeneous chemical steps coupled to the electron transfer are formally similar to the equation describing the diffusion to partially blocked electrodes[30,31,36], so it can be envisaged that the gramicidin structures on the phospholipid monolayer can behave as active pinholes embedded in a blocked phospholipid film. This possibility was initially considered as negligible[46–48,52,55] because the small size of gramicidin channels in biological membranes (cross section around 2 square nanometers[51]). However, the structure of gramicidin in supported lipid films is not clear yet, and the possibility of gramicidin aggregates of higher dimensions acting as active centers cannot be discarded. Recently, the impedance method has been applied to the system in order to decide if it can be described according to the model of partially blocked electrodes[58].

The analysis of the impedance data with the frequency at potentials along the reduction wave was done according to Eq. (*16*). As shown in Fig. 5, the plots Z_F' or Z_F'' vs $\omega^{-1/2}$ are characteristic for an electron transfer on partially blocked electrodes, according to Eq. (*16*). A suitable analysis of the experimental data can provide the four characteristic parameters: R_{ct}, σ, $(1 - \theta)$ and q. The analysis procedure used in ref.[58] consist in obtaining a first estimation of σ and θ from the slopes at low and high frequency limits,

and with these values, a first estimation of R_{ct} from the electrode admittance, Y_{el}', at high frequencies according to the expression for the high frequency limit:

$$Y'_{el} = \frac{\omega^{1/2}}{(\sigma)_{app}} \frac{(p')_{app}\,\omega^{1/2} + 1}{((p')_{app}\,\omega^{1/2} + 1)^2 + 1} \tag{21}$$

with $(\sigma)_{app}$ defined in Eq. (*18b*) and

$$(p')_{app} = \frac{p'}{2 - \theta} \tag{22}$$

being p' the irreversibility quotient defined as $p' = R_{ct}/\sigma$.

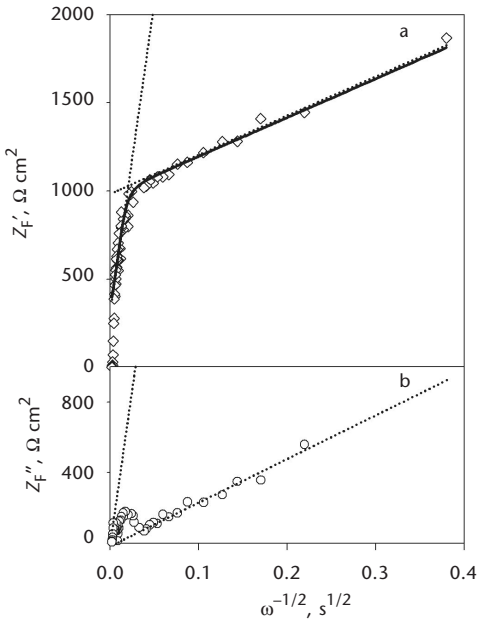

FIG. 5
Z_F' vs $\omega^{-1/2}$ (a) and Z_F'' vs $\omega^{-1/2}$ (b) plots obtained with the gramicidin-modified DOPC coated mercury electrode in the supporting electrolyte solution containing 10^{-4} M Tl^+ at –0.440 V. The dotted lines correspond to the linear regressions over the values at the high frequency and at low frequency limits. The solid line corresponds to the curve generated with the parameters obtained from the fitting procedure: σ = 2200 Ω cm^2 s$^{-1/2}$, R_{ct} = 27 Ω cm^2, (1 – θ) = 0.08, q = 3500 s^{-1}. With permission from *J. Electroanal. Chem.* **2010**, *649*, 42

Then, the estimated values of R_{ct}, σ, θ and q are used as initial parameters in a fitting procedure on the real components of the faradaic impedance and of the electrode admittance at every dc potential within the faradaic region. The quality of the fitting can be observed in Figs 5 and 6.

The values of (1 – θ) obtained from this analysis are in the range of 0.06–0.1 at potentials around the centre of the faradaic signal. R_a values are 0.9–1 micrometers. Therefore, using these values and Eq. (*17b*), R_0 values around 3–5 micrometers can be calculated. These results are consistent with the model assumptions about low active sites coverage but evidently, they do not agree with a model consisting in a random distribution of single gramicidin channels along the film. For instance, the area of a single gramicidin channel is ca. 2 nm^2, quite different from the calculated area for an active centre, 3 μm^2. However, STM studies of gramicidin inserted in phospholipid films[59] provide a model of gramicidin molecules surrounded by at least one layer of bound phospholipid forming units that are not homogeneously distributed on the film, but accumulated on areas all along the surface. Those areas may act as active sites for the Tl(I) reduction, explaining the values of the geometric parameters obtained from the impedance analysis. It is expected that all the aggregates will not have the same

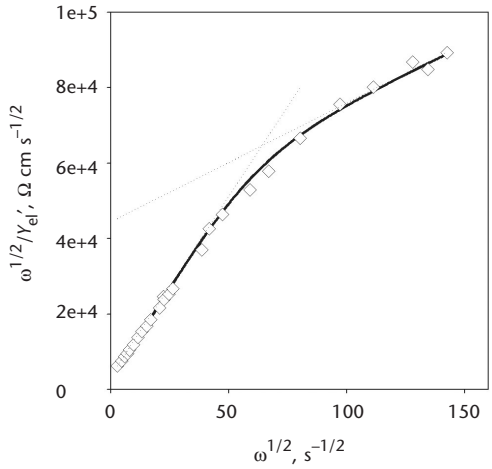

FIG. 6
$\omega^{1/2}/Y_{el}'$ vs $\omega^{1/2}$ plot obtained with the gramicidin-modified DOPC coated mercury electrode in the supporting electrolyte solution containing 10^{-4} M Tl^+ at E = –0.440 V. The dotted lines correspond to the linear regressions over the values at the high frequency and at low frequency limits. The solid line corresponds to the curve generated with the parameters obtained from the fitting procedure: σ = 2200 Ω cm^2 $s^{-1/2}$, R_{ct} = 27 Ω cm^2, (1 – θ) = 0.08, q = 3500 s^{-1}. With permission from *J. Electroanal. Chem.* **2010**, *649*, 42

area, but a distribution of active sites areas , as was done by Compton and co-workers for the voltammetric analysis[32–34] has not yet be considered in the impedance equations.

In addition to the geometric information contained in the parameters θ and q, the analysis with the frequency provides the parameters of the faradaic reaction, σ, R_{ct} and p', which include in their definitions kinetic information about the electron transfer. Thus, the σ vs E plot, shown in Fig. 7, conforms well the curve corresponding to a dc reversible electron transfer with the parameters for Tl(I) reduction (D = 1.85 × 10^{-5} cm^2 s^{-1}, E^0 = –0.455 V vs SCE[56,57]).

Moreover, the irreversibility coefficient, p', provides the forward rate constant of the electron transfer at every dc potential, according to the Eq. (*23*):

$$k_f = \frac{2^{1/2} D^{1/2}}{p'(1+\exp\varphi)} \qquad (23)$$

with φ being the dimensionless potential φ = (nF/RT)(E – E^0).

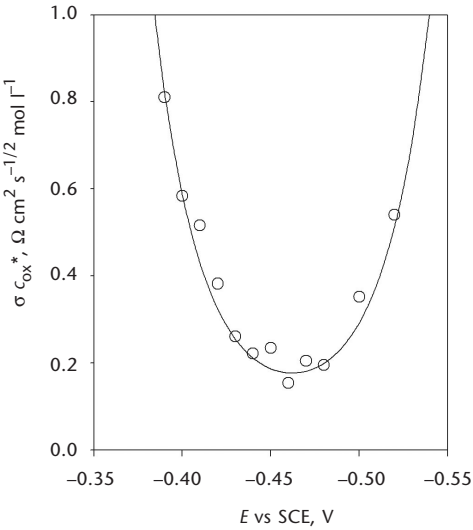

FIG. 7

The Warburg coefficient (σ) as a function of potential obtained from the analysis with the frequency of the impedance data on a gramicidin-modified DOPC coated mercury electrode in the supporting electrolyte solution containing 10^{-4} M Tl^+. The solid line represents the theoretical values generated for a dc-reversible one-electron transfer and D_{ox} = 1.85 × 10^{-5} cm^2 s^{-1}, E^o = –0.455 V. With permission from *J. Electroanal. Chem.* **2010**, *649*, 42

The ln k_f vs φ plot shown in Fig. 8 can be considered linear. From the slope and the intercept the charge transfer coefficient, α, and the standard rate constant, k^s, for the reduction have been obtained. The values are 0.62 and 0.09 cm s^{-1}, respectively. The value for α is not far from the generally adopted value for an elemental electron transfer, however the k^s value is much lower than 1.2 cm s^{-1}, value of k^s obtained with uncoated mercury electrodes[56,57]. This can indicate some contribution of the translocation of the ion through the interior of the gramicidin channel to the rate of the process[55].

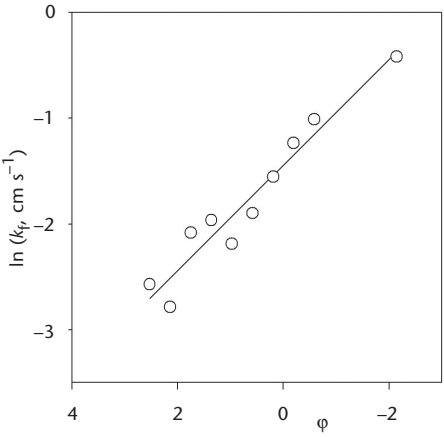

FIG. 8
ln k_f vs φ curve for the Tl^+ reduction on a gramicidin-modified DOPC coated mercury electrode in the supporting electrolyte solution containing 10^{-4} M Tl^+. The solid line corresponds to the linear regression over the data. With permission from *J. Electroanal. Chem.* **2010**, *649*, 42

4. A SURFACE CONFINED REDOX REACTION

In a surface confined redox reaction the diffusional mass transport is negligible because both the reactant and the product are strongly adsorbed[60–63]. These reactions are frequently present in studies of redox sites embedded in self assembled monolayers[64–66], and have received great attention because of their application in sensing technologies.

Laviron developed the equations corresponding to this kind of reaction for voltammetry[67], ac polarography and faradaic impedance techniques[68], assuming a Langmuir isotherm[69] or a Frumkin isotherm[70]. O'Dea and Osteryoung[71], and Mirčeski[72] applied the square wave voltammetry to this kind of reactions while Molina and González[73–75] applied multi-step

potentiostatic techniques, and Wang et al.[76] used Fourier transformed square-wave voltammetry. The application of these methods under particular experimental conditions can provide values for the standard rate constant and the charge transfer coefficient of the redox process. Recently, Rueda et al.[77] have extended the application of impedance spectroscopy to surface confined redox reaction, including both the influence of the frequency and of the dc potential.

4.1. Impedance of a Surface Confined Redox Reaction

The current density corresponding to a surface faradaic reaction without mass transport effects and in the absence of interactions between adsorbed species can be exclusively expressed in terms of the surface concentrations of oxidized and reduced species[78]:

$$j_F = -nF(k_{f,\Gamma}\Gamma_{Ox} - k_{b,\Gamma}\Gamma_{Red}) \,. \tag{24}$$

The forwards and backwards first order rate constants of the surface reaction, $k_{f,\Gamma}$ and $k_{b,\Gamma}$, are expected to behave with the potential according to the Butler–Volmer equation:

$$k_{f,\Gamma} = k_j e^{-\alpha\varphi} \tag{25a}$$

$$k_{b,\Gamma} = k_j e^{(1-\alpha)\varphi} \tag{25b}$$

$k_{f,\Gamma}$ and $k_{b,\Gamma}$ are coincident at the equilibrium potential, E^j, that depends on the standard potential and on the adsorption equilibrium of reactant and products. The coincident value of $k_{f,\Gamma}$ and $k_{b,\Gamma}$ at E^j, k_j, can be considered a pseudo-standard rate constant of the surface reaction. The dimensionless potential, φ, is then referred to E^j:

$$\varphi = \frac{nF}{RT}(E - E^j) \,. \tag{26}$$

The definition of the faradaic current density given in Eq. (*24*) permits to obtain the frequency dependence of the faradaic impedance[68–70]:

$$Z_F = R_{ct} + \frac{1}{i\omega C_a} \,. \tag{27}$$

R_{ct} and C_a are the charge transfer resistance and the adsorption capacitance, which include kinetic information in their definitions.

$$R_{ct} = \left(\frac{\partial j}{\partial E}\right)^{-1}_{\Gamma_i} = \frac{RT}{n^2 F^2 k_{f,\Gamma}} \frac{1}{\alpha\Gamma_{Ox} + (1-\alpha)\Gamma_{Red} e^{\varphi}} \tag{28}$$

$$C_a = nF\left[\left(\frac{\partial E}{\partial \Gamma_{Ox}}\right)_{j,\Gamma_{Red}} - \left(\frac{\partial E}{\partial \Gamma_{Red}}\right)_{j,\Gamma_{Ox}}\right]^{-1} = \frac{n^2 F^2}{RT} \frac{\alpha\Gamma_{Ox} + (1-\alpha)\Gamma_{Red} e^{\varphi}}{1 + e^{\varphi}} \tag{29}$$

The electrochemical cell impedance includes the faradaic contribution in parallel to the double layer impedance characterized by a high frequency capacitance, C_{HF}, and the ohmic resistance of the electrolyte, R_S. Then, the frequency dependence of the electrochemical impedance of the cell becomes:

$$Z = R_s + \cfrac{1}{C_{HF} i\omega + \cfrac{1}{R_{ct} + \cfrac{1}{C_a i\omega}}} \tag{30}$$

with C_{HF} defined as:

$$C_{HF} = \left(\frac{\partial \sigma^M}{\partial E}\right)_{\Gamma_i} . \tag{31}$$

Therefore, the electrochemical cell can be represented by the equivalent circuit in Scheme 2.

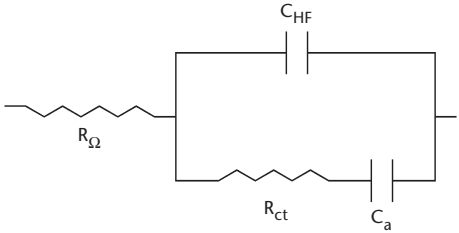

SCHEME 2
Equivalent circuit representing the electrochemical cell during a surface confined reaction. With permission from *Electrochim. Acta*, in press, doi:10.1016/j.electacta.2010.12.061

4.2. Example: The Reduction of Azobenzene on Mercury

The reduction of azobenzene to hydrazobenzene is a representative surface confined reaction due to the strong adsorption of the species involved[61,79,80]. Then, it has been used by several authors to check the applicability of different electrochemical techniques to the study of reactions in the absence of diffusion[60,61,67–82]. Laviron[67] performed a complete voltammetric study of this reaction at a wide range of pH, obtaining the standard rate constant as a function of the pH.

In a previous paper, the Electrochemical Impedance Spectroscopy was applied to azobenzene reduction at pH 4.18–5.25 [77]. The pH dependence of the equilibrium potential, E^{j}, suggests the participation of two protons in the bielectronic reduction of azobenzene. The complex plane plots of the impedance at potentials within the faradaic region, as the one shown in Fig. 9, are characteristic of a difussionless faradaic process: a circular arc, at high frequencies mainly originated by the faradaic impedance and a pure capacitative vertical line at low frequencies. At potentials far negative (–0.35 V in the figure) or positive (–0.1 V in the figure) a pure capacitative behavior is obtained. A linear trend with a slope of 45°, characteristic of mass transport is not present at any potential or pH investigated.

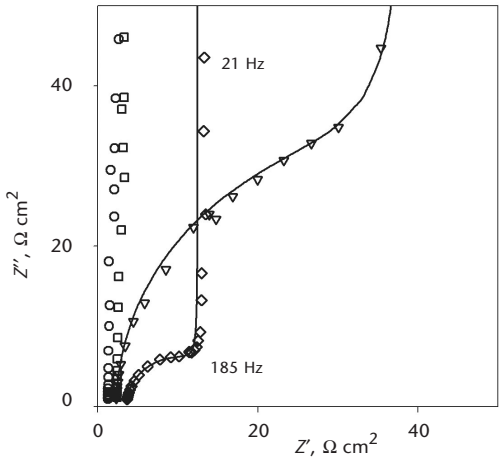

FIG. 9

Complex plane plots of the experimental impedance spectra obtained in a solution of 10^{-6} M azobenzene at pH 5.25 and different potentials: –0.1 V (○), –0.26 V (△) and –0.35 V (□) and at pH 4.18 and –0.19 V (◇). The lines represent the generated curves with the parameters obtained in the analysis as a function of the frequency. With permission from *Electrochim. Acta*, in press, doi:10.1016/j.electacta.2010.12.061

For the evaluation of the four parameters R_S, C_{HF}, R_{ct} and C_a at every dc potential within the faradaic region a fitting procedure based on the frequency dependence of the real and imaginary components of the electrode admittance was used. Effectively, after correction of the ohmic resistance, the real and imaginary components of the electrode impedance according to Eq. (*30*) can be combined to yield the real and imaginary components of the electrode admittance. Their expressions as a function of the frequency are given in Eqs (*32*).

$$Y'_{el} = \frac{R_{ct} C_a^2 \omega^2}{1 + R_{ct}^2 C_a^2 \omega^2} \tag{32a}$$

$$Y''_{el} = \frac{R_{ct} \omega}{1 + R_{ct}^2 C_a^2 \omega^2} + C_{HF} \omega \tag{32b}$$

This analysis does not require an "a priori" correction of the double layer capacitance. The values of R_{ct} and C_a obtained from this analysis at every dc potential include the surface concentrations of reactant and product. To separate its influence from the kinetic information, C_a and R_{ct} are combined to yield the forward rate constant of the surface process:

$$k_{f,\Gamma} = \frac{1}{R_{ct} C_a (1 + e^{\varphi})} \,. \tag{33}$$

Plots of ln $k_{f,\Gamma}$ vs E at different pH values are shown in Fig. 10. It can be observed that the plots shift towards more negative potentials as the pH increases, as can be expected from the participation of two protons. At constant pH, ln $k_{f,\Gamma}$ vs E plots exhibit clear deviations from linearity that cannot be explained on the basis of the Butler–Volmer equation, that would apply in the case of kinetic control by an elementary step. In order to explain this deviation, a sequential reactions schemes was considered that includes at least two protonations and two electron transfers steps. A general sequential CECEC mechanism, with 'C' representing a chemical step and 'E' an electron transfer step takes into account all positions of the chemical steps with respect to the two electron transfer steps.

The potential dependence of the forward rate constant of the overall process for this mechanism can be easily obtained under the steady state assumption for the surface concentrations of every intermediate species[83]:

$$\frac{1}{k_{f,\Gamma}} = \frac{1}{B_0} + \frac{\exp\left(\frac{1}{4}\varphi'\right)}{A_1} + \frac{\exp\left(\frac{1}{2}\varphi'\right)}{B_1} + \frac{\exp\left(\frac{3}{4}\varphi'\right)}{A_2} + \frac{\exp\varphi'}{B_2} \qquad (34)$$

The coefficients B_i and A_i include the kinetic rate constants of the chemical steps and the electron transfer steps respectively and the thermodynamic constants of previous steps. In Eq. (*34*) the dimensionless potential, φ′, is referenced to an arbitrary potential (E' = –0.25 V vs SCE in the data of Fig. 10).

The slopes of ln $k_{f,\Gamma}$ vs E correspond to α values ranging from 0.75 at the less negative potentials to 0.35–0.5 at more negative potentials. According to Eq. (*34*), the value of α = 0.75 suggests that the second electron transfer is rate controlling, while α = 0.35–0.5 indicates rate control by the first electron transfer or by a chemical step between both electron transfers. Therefore, two possible particular sequences can be considered.

First an eCE mechanism, with a chemical step after the first electron transfer and the second electron transfer controlling the rate of the overall process. The lowercase 'e' indicates the non controlling character of the

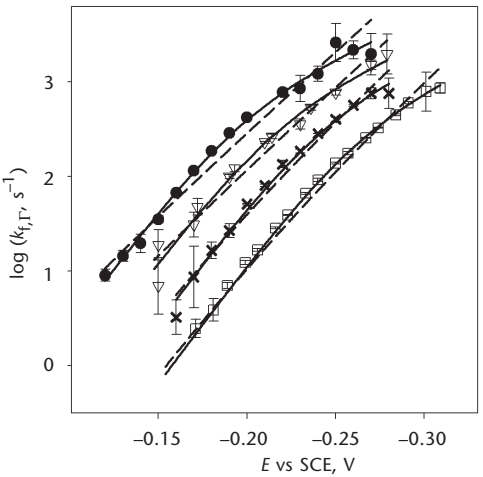

FIG. 10
log $k_{f,\Gamma}$ vs E plots calculated with Eq. (*33*) and the values of R_{ct} and C_a obtained with solutions of 2 × 10^{-6} M azobenzene at pH 4.18 (●), 10^{-6} M at pH 4.6 (△), 2 × 10^{-6} at pH 4.9 (×) and 2 × 10^{-6} M at pH 5.25 (□). Theoretical values corresponding to the best fit to an eCE mechanism, Eq. (*35*), (– – –) and to an EE mechanism, Eq. (*36*), (——). With permission from *Electrochim. Acta*, in press, doi:10.1016/j.electacta.2010.12.061

first electron transfer step. The potential dependence of log $k_{f,\Gamma}$ in Eq. (*34*) can then be simplified as:

$$\frac{1}{k_{f,\Gamma}} = \frac{\exp\left(\frac{1}{2}\varphi'\right)}{B_1} + \frac{\exp\left(\frac{3}{4}\varphi'\right)}{A_2} . \qquad (35)$$

The second particular sequence to be considered is an EE mechanism with both electron transfer steps controlling the rate of the overall process. In this case only the second and fourth terms of the general expression (Eq. (*34*)) have to be included in the rate constant expression:

$$\frac{1}{k_{f,\Gamma}} = \frac{\exp\left(\frac{1}{4}\varphi'\right)}{A_1} + \frac{\exp\left(\frac{3}{4}\varphi'\right)}{A_2} . \qquad (36)$$

In Fig. 10 it can be observed that the best fit of the experimental data to Eq. (36) suggests that both electron transfers are rate controlling. The values of the kinetics parameters A_1 and A_2 are obtained from the analysis of k_f as a function of potential at all the experimental pH conditions. Then, the analysis of A and A_2 as a function of pH can provide information concerning the chemical steps, because they contain the equilibrium constants of previous steps.

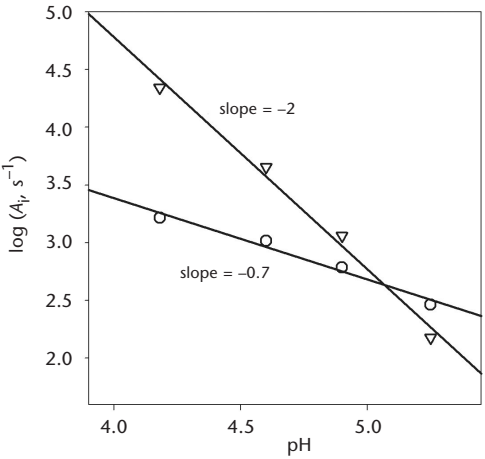

FIG. 11
Variations with the pH of the kinetics parameters corresponding to an EE mechanism, log A_1 (○) and log A_2 (△). The solid lines correspond to the linear regressions. With permission from *Electrochim. Acta*, in press, doi:10.1016/j.electacta.2010.12.061

Plots of log A_1 and log A_2 vs pH are shown in Fig. 11. They exhibit a linear trend with slopes of –0.7 and –2.0, respectively. From these values the existence of two proton transfers previous to the second electron transfer, with one of them preceding the first electron transfer, is concluded.

In summary, the main reaction pathway is consistent with a cEcE mechanism (Scheme 3) which includes a protonation step before the first electron transfer and a second protonation step preceding the second electron transfer. Both protonations are fast and both electron transfers are rate controlling.

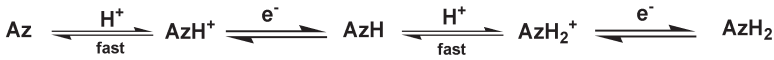

SCHEME 3

Multistep mechanism proposed for the reduction of azobenzene (Az) to hydrazobenzene (AzH_2) on mercury in the absence of diffusion. With permission from E*lectrochim. Acta*, in press, doi:10.1016/j.electacta.2010.12.061

5. GENERAL CONCLUSIONS

In this review it has been shown that Electrochemical Impedance Spectroscopy is a powerful tool in the study of surface electrode processes. The capability of EIS to separate different contributions to the overall electrochemical response and the wide range of time windows covered in the frequency scan permits to obtain kinetic information inaccessible by other techniques. In addition, the study of the influence of the dc potential on the parameters obtained from the frequency analysis provides a deeper picture of the surface processes.

These conclusions are confirmed with three selected examples of surface processes:

The adsorption of adenine on Au(111) from NaF solutions exhibit a mixed kinetic control by diffusion and by adsorption steps. The corresponding relaxation times and rate constants have been calculated.

The reduction of Tl(I) on gramicidin modified DOPC coated mercury electrodes differs from the reduction on bare mercury, and its behaviour can be explained according to a diffusion model to a partially blocked electrode. This situation would be in accordance with the formation of aggregates of gramicidin channel–phospholipid units on the film, that may act as active sites for Tl(I) reduction. Moreover, the rate constant obtained for the Tl(I) reduction suggests the contribution of the translocation of the ion trough the channel to the rate of the process.

Finally, the reduction of azobenzene to hydrazobenzene on mercury electrodes from acid solutions and in the absence of mass transport effects follows a cEcE mechanism, with a fast protonation preceding each rate determining electron transfer step. The kinetic parameters of both electron transfers have been determined.

6. LIST OF SYMBOLS

c (mol m^{-3})	concentration
C_a (F m^{-2})	adsorption capacitance in surface confined electrode reaction
C_{ad} (F m^{-2})	capacity of the adsorption process
C_d (F m^{-2})	differential double layer capacity
C_{HF} (F m^{-2})	high frequency capacitance
$c_{x=0}$ (mol m^{-3})	concentration at the electrode surface
D (m^2 s^{-1})	diffusion coefficient
E (V vs SCE)	electrode potential
E^0 (V vs SCE)	standard potential
E^j (V vs SCE)	equilibrium potential of a surface confined electrode reaction
$g^{\neq}$	interaction parameter of the activated complex in an adsorption step
i	complex unit, $(-1)^{1/2}$
j (A m^{-2})	total current density
j_{ad} (A m^{-2})	current density due to the adsorption phenomena
j_c (A m^{-2})	capacitative current density
j_F (A cm^{-2})	faradaic current density due to a surface confined electrode reaction
k_{ad} (m s^{-1})	rate constant of the adsorption step
$k_{ad}f_{ad}(\Gamma)$ (m s^{-1})	specific rate of adsorption
k_b (m s^{-1})	oxidation rate constant of an electrode reaction
$k_{b,\Gamma}$ (s^{-1})	oxidation rate constant of a surface confined electrode reaction
k_d (m s^{-1})	rate constant of the desorption step
$k_df_d(\Gamma)$ (m s^{-1})	specific rate of desorption
k_f (m s^{-1})	reduction rate constant of an electrode reaction
$k_{f,\Gamma}$ (s^{-1})	reduction rate constant of a surface confined electrode reaction
k_j (s^{-1})	pseudo-standard rate constant of surface confined electrode reaction
n	stochiometric number of electrons in an electrode process
p' (s$^{1/2}$)	irreversibility quotient, defined as R_{ct}/σ
$(p')_{app}$ (s$^{1/2}$)	apparent irreversibility quotient, defined as $(R_{ct})_{app}/(\sigma)_{app}$
R_0 (m)	radius of inactive areas surrounding active pinholes
R_a (m)	radius of active pinholes
R_{ad} (Ω m^2)	adsorption resistance
R_{ct} (Ω cm^{-2})	charge transfer resistance
$(R_{ct})_{app}$ (Ω m^{-2})	apparent charge transfer resistance
R_S (Ω m^2)	solution resistance
t (s)	time
v (mol m^{-2} s^{-1})	net rate of a surface process
Y_{el}' (Ω^{-1} m^{-2})	real component of the electrode admittance
Y_{el}'' (Ω^{-1} m^{-2})	imaginary component of the electrode admittance

Z_{ad} (Ω m^2)	adsorption impedance
Z_{cel} (Ω m^2)	electrochemical cell impedance
Z_F' (Ω m^2)	real component of the faradaic impedance
Z_F'' (Ω m^2)	imaginary component of the faradaic impedance
α	charge transfer coefficient
γ	electrosorption valency
Γ (mol m^{-2})	surface excess
Γ_m (mol m^{-2})	maximum surface excess
Γ_{Ox} (mol m^{-2})	surface concentration of oxidized species
Γ_{Red} (mol m^{-2})	surface concentration of reduced species
φ	dimensionless potential defined as $\varphi = (nF/RT)(E - E^0)$.
φ'	dimensionless potential referenced to an arbitrary potential, E', defined as $\varphi' = (nF/RT)(E - E')$
μ_{ad} (J mol^{-1})	chemical potential of adsorbed species
μ_S (J mol^{-1})	chemical potential of species in solution
μ_S^0 (J mol^{-1})	standard chemical potential of species in solution
θ	coverage
σ (Ω m^2 s$^{-1/2}$)	Warburg coefficient
σ_{ad} (Ω m^2 s$^{-1/2}$)	Warburg coefficient of adsorption process
$(\sigma)_{app}$ (Ω m^2 s$^{-1/2}$)	apparent Warburg coefficient
σ^M (C m^{-2})	surface charge density
τ_D (s)	relaxation time of diffusion
τ_H (s)	relaxation time of adsorption
ω (s^{-1})	angular frequency

*Financial support from Ministerio de Ciencia e Innovación (Spain) (Projects CTQ2004-06645/BQU and CTQ2010-**19823**) and Junta de Andalucia (Grupo FQM202) is greatly acknowledged.*

7. REFERENCES

1. Sluyters-Rehbach M., Sluyters J. H.: *Rec. Trav. Chim. Pays-Bas* **1963**, *82*, 525.
2. Smith D. E.: *Anal. Chem.* **1963**, *35*, 602.
3. Timmer B., Sluyters-Rehbach M., Sluyters J. H.: *J. Electroanal. Chem.* **1967**, *14*, 169
4. Sluyters-Rehbach M., Sluyters J. H. in: *Comprehensive Treatise of Electrochemistry* (E. Yeager, Ed.), Vol. 9, p. 177. Plenum Press, New York 1984.
5. Sluyters-Rehbach M., Sluyters J. H. in: *Electroanalytical Chemistry* (A. J. Bard, Ed.), Vol. 4, p. 1. Marcel Dekker, New York 1970.
6. Sluyters-Rehbach M., Sluyters J. H. in: *Chemical Kinetics* (C. H. Bamford and R. G. Compton, Eds), Vol. 26, p. 349. Elsevier, Amsterdam 1986.
7. Smith D. E. in: *Electroanalytical Chemistry* (A. J. Bard, Ed.), Vol. 1, p. 1. Marcel Dekker, New York 1966.
8. Epelboin I., Gabrielli C., Keddam M. in: *Comprehensive Treatise of Electrochemistry* (E. Yeager, Ed.), Vol. 9, p. 61. Plenum Press, New York 1984.
9. Macdonald J. R.: *Impedance Spectroscopy*. Wiley, New York 1984.
10. Orazem M. E., Tribollet B.: *Electrochemical Impedance Spectroscopy*. Wiley, New York 2008.

11. Rueda M. in: *Research in Chemical Kinetics* (R. G. Compton and G. Hancock, Eds), Vol. 4, p. 31. Blackwell Science ltd., Oxford 1997.
12. Pajkossy T.: *J. Electroanal. Chem.* **1994**, *364*, 111.
13. de Levie R.: *Electrochim. Acta* **1965**, *10*, 113.
14. Nguyen Van Huong C., Hinnen C., Dalbera J. P., Parsons R.: *J. Electroanal. Chem.* **1982**, *125*, 177.
15. Lipkowski J., Nguyen Van Huong C., Hinnen C., Parsons R., Chevalet J.: *J. Electroanal. Chem.* **1983**, *143*, 375.
16. Jović V. D., Parsons R., Jović B. M.: *J. Electroanal. Chem.* **1992**, *339*, 327.
17. Frumkin A., Melik-Gaikazyan V. I.: *Dokl. Akad. Nauk U.S.S.R.* **1952**, *26*, 560.
18. Retter U., Jehring H.: *J. Electroanal. Chem., Interfacial Electrochem.* **1973**, *46*, 375.
19. Berzins T., Delahay P.: *J. Phys. Chem.* **1955**, *59*, 906.
20. Pajkossy T., Wandlowski T., Kolb D. M.: *J. Electroanal. Chem.* **1996**, *414*, 209.
21. Eberhardt D., Santos E., Schmickler W.: *J. Electroanal. Chem.* **1996**, *419*, 23.
22. Pajkossy T.: *Solid State Ionics* **1997**, *94*, 123.
23. Kerner Z., Pajkossy T.: *Electrochim. Acta* **2002**, *47*, 2055.
24. Sluyters-Rehbach M.: *Pure Appl. Chem.* **1994**, *66*, 1831.
25. Prado C., Prieto F., Rueda M., Feliu J., Aldaz A.: *Electrochim. Acta* **2007**, *52*, 3168.
26. Prieto F., Rueda M., Prado C., Feliu J., Aldaz A.: *Electrochim. Acta* **2010**, *55*, 3301.
27. a) Szulborska A., Baranski A.: *J. Electroanal. Chem.* **1994**, *377*, 23; b) Szulborska A., Baranski A: *J. Electroanal. Chem.* **1994**, *377*, 269.
28. Vetter K. J.: *Z. Phys. Chem.* **1952**, *199*, 300.
29. Jehring H., Retter U., Horn E.: *J. Electroanal. Chem.* **1983**, *149*, 153.
30. Tokuda K., Gueshi T., Matsuda H.: *J. Electroanal. Chem.* **1979**, *102*, 41.
31. Amatore C., Saveant J. M., Tessier D.: *J. Electroanal. Chem.* **1983**, *147*, 39.
32. Davies T. J., Banks C. E., Compton R. G.: *J. Solid State Electrochem.* **2005**, *9*, 797.
33. Davies T. J., Compton R. G.: *J. Electroanal. Chem.* **2005**, *585*, 63.
34. Davies T. J., Ward-Jones S., Banks C. E., Del Campo J., Mas R., Muñoz F. X., Compton R. G.: *J. Electroanal. Chem.* **2005**, *585*, 51.
35. Menshykau D., Compton R. G.: *Langmuir* **2009**, *25*, 2519.
36. Finklea H. O., Snider D. A., Fedyk J., Sabatani E., Gafni Y., Rubinstein I.: *Langmuir* **1993**, *9*, 3660.
37. Miller I. R. in: *Topics in Bioelectrochemistry and Bioenergetics* (G. Milazzo, Ed.), Vol. 4, p. 161. John Wiley and Sons, Chichester 1981.
38. Nelson A., Benton A.: *J. Electroanal. Chem.* **1986**, *202*, 253.
39. Nelson A., Auffret N.: *J. Electroanal. Chem.* **1988**, *244*, 99.
40. Nelson A., Auffret N.: *J. Electroanal. Chem.* **1988**, *248*, 167.
41. Nelson A., Auffret N., Borlakoglu J.: *Biochim. Biophys. Acta* **1990**, *1021*, 205.
42. Nelson A.: *J. Electroanal. Chem.* **1991**, *303*, 221.
43. Nelson A.: *J. Chem. Soc., Faraday Trans.* **1993**, *89*, 2799.
44. Nelson A.: *Langmuir* **1996**, *12*, 2058.
45. Nelson A.: *Langmuir* **1997**, *13*, 5644.
46. Nelson A., Bizzotto D.: *Langmuir* **1999**, *15*, 7031.
47. Nelson A.: *Biophys. J.* **2001**, *80*, 2694.
48. Rueda M., Navarro I., Ramirez G., Prieto F., Prado C., Nelson A.: *Langmuir* **1999**, *15*, 3672.
49. Roux B., Karplus M.: *Annu. Rev. Biophys. Biomol. Struct.* **1994**, *23*, 731.

50. Roux B., Prodhom B., Karplus M.: *Biophys. J.* **1995**, *68*, 876.
51. Urry D. W.: *Proc. Natl. Acad. Sci. U.S.A.* **1971**, *68*, 672.
52. Rueda M., Navarro I., Prado C., Silva C.: *J. Electrochem. Soc.* **2001**, *148*, E139.
53. Mauzeroll J., Buda M., Bard A. J., Prieto F., Rueda M.: *Langmuir* **2002**, *18*, 9453.
54. Prieto F., Navarro I., Rueda M.: *J. Electroanal. Chem.* **2003**, *550–551*, 253.
55. Becucci L., Moncelli M. R., Guidelli R.: *Biophys. J.* **2002**, *82*, 852.
56. Sluyters-Rehbach M., Timmer B., Sluyters J. H.: *Rec. Trav. Chim. Pays-Bas* **1963**, *82*, 553.
57. Blankenborg S. G. J., Sluyters-Rehbach M., Sluyters J. H.: *J. Electroanal. Chem.* **1993**, *349*, 255.
58. Rueda M., Prieto F., Navarro I., Romero R.: *J. Electroanal. Chem.* **2010**, *649*, 42.
59. Sek S., Laredo T., Dutcher J. R., Lipkowski J.: *J. Am. Chem. Soc.* **2009**, *131*, 6439.
60. Lovric M., Komorsky-Lovric S., Branica M.: *Croat. Chem. Acta* **1993**, *66*, 279.
61. Komorsky-Lovric S., Lovric M.: *Electrochim. Acta* **1995**, *40*, 1781.
62. Mirčeski V., Lovric M.: *Electroanalysis* **1997**, *9*, 1283.
63. Komorsky-Lovric S.: *J. Electroanal. Chem.* **2000**, *482*, 222.
64. Finklea H. O., Yoon K., Chamberlain E., Allen J., Haddox R.: *J. Phys. Chem. B* **2001**, *105*, 3088.
65. Smalley J. F.: *J. Phys. Chem. B* **2007**, *111*, 6798.
66. Wijma H. J., Jeuken L. J. C., Verbeet M. P., Armstrong F. A., Canters G. W.: *J. Am. Chem. Soc.* **2007**, *129*, 8557.
67. Laviron E., Mugnier Y.: *J. Electroanal. Chem.* **1980**, *111*, 337.
68. Laviron E.: *J. Electroanal. Chem.* **1979**, *97*, 135.
69. Laviron E.: *J. Electroanal. Chem.* **1979**, *105*, 25.
70. Laviron E.: *J. Electroanal. Chem.* **1979**, *105*, 35.
71. O'Dea J. J., Osteryoung J. G.: *Anal. Chem.* **1993**, *65*, 3090.
72. Mirčeski V.: *J. Electroanal. Chem.* **2001**, *508*, 138.
73. González J., Molina A.: *Langmuir* **2001**, *17*, 5520.
74. Molina A., González J.: *Langmuir* **2003**, *19*, 406.
75. Molina A., González J.: *J. Electroanal. Chem.* **2005**, *585*, 132.
76. Wang L., Chen H., Huang X., Nan J.: *Electroanalysis* **2009**, *21*, 755.
77. Prieto F., Rueda M., Hidalgo J., Martínez E., Navarro I.: *Electrochim. Acta* **2011**, in press, doi:10.1016/j.electacta.2010.12.061.
78. Laviron E.: *J. Electroanal. Chem.* **1979**, *101*, 19.
79. Wopschall R. H., Shain I.: *Anal. Chem.* **1967**, *39*, 1535.
80. Schwarz W. M., Shain I.: *J. Phys. Chem.* **1965**, *69*, 30.
81. Komorsky-Lovric S., Lovric M.: *J. Electroanal. Chem.* **1995**, *384*, 115.
82. Mirsceski V., Gulaboshi R.: *J. Solid State Chem.* **2003**, *7*, 157.
83. Navarro I., Prieto F., Rueda M.: *J. Electroanal. Chem.* **1994**, *366*, 127.